Structural and functional modularity of voltage-gated potassium channels

Craig D. Patten[a,b,*], Marco Caprini[b,1], Rosa Planells-Cases[b,c,2], Mauricio Montal[b,3]

[a] *Department of Physics, University of California at San Diego, La Jolla, CA 92093, USA*
[b] *Department of Biology, University of California at San Diego, La Jolla, CA 92093, USA*
[c] *Department of Neuroscience, University of California at San Diego, La Jolla, CA 92093, USA*

Received 22 October 1999; received in revised form 22 November 1999

Edited by Giorgio Semenza

Abstract Sequence similarity among known potassium channels indicates the voltage-gated potassium channels consist of two modules: the N-terminal portion of the channel up to and including transmembrane segment S4, called in this paper the 'sensor' module, and the C-terminal portion from transmembrane segment S5 onwards, called the 'pore' module. We investigated the functional role of these modules by constructing chimeric channels which combine the 'sensor' from one native voltage-gated channel, mKv1.1, with the 'pore' from another, *Shaker* H4, and vice versa. Functional studies of the wild type and chimeric channels show that these modules can operate outside their native context. Each channel has a unique conductance–voltage relation. Channels incorporating the mKv1.1 sensor module have similar rates of activation while channels having the *Shaker* pore module show similar rates of deactivation. This observation suggests the mKv1.1 sensor module limits activation and the *Shaker* pore module determines deactivation. We propose a model that explains the observed equilibrium and kinetic properties of the chimeric constructs in terms of the characteristics of the native modules and a novel type of intrasubunit cooperativity. The properties ascribed to the modules are the same whether the modules function in their native context or have been assembled into a chimera.

Key words: Potassium channel; Structure–activity relationship; Modularity; Ion channel kinetics

1. Introduction

The sequence similarity between voltage-gated potassium channels and voltage-gated sodium or calcium channels suggested a modular architecture of the voltage-gated ion channel family. The first potassium channel cloned from the *Drosophila Shaker* locus [1] seemed to encode one module similar to one of the four internal repeats of the more complex sodium or calcium channel [2,3]. Examination of the sequence of subsequently cloned potassium channels from diverse sources indicates that there may be a further modularity within the voltage-gated potassium channels [4–6]. The genes encoding the inward rectifier class of potassium channels encode a protein homologous to the carboxy-terminal portion of the voltage-gated potassium channels, the S5-H5-S6 region [7]. These genes are sufficient to form potassium-selective pores, but with little intrinsic voltage sensitivity. As such, the S5-H5-S6 region of voltage-gated channels may represent a 'pore' module within the larger protein. Crystallization of the *Streptomyces lividans* KcsA protein has provided a structure for such a pore module [8,9]. Meanwhile many of the voltage-dependent properties of the voltage-gated potassium channels have been attributed to the amino-terminal half of the protein, notably the S4 transmembrane segment [10–14], and the cluster comprised by transmembrane segments S2, S3, and S4 [15–18]. The amino-terminal portion of the protein may thus represent a 'sensor' module, responsible for detecting changes in transmembrane potential. Furthermore, potassium channels have been discovered that are constructed from two 'pore' modules with [19] or without [20] an attached 'sensor' module. Thus it appears reasonable that voltage-gated potassium channels are structurally modular. We examined this hypothesis by constructing chimeric voltage-gated potassium channels using the modules from the *Shaker* H4 channel (ShH4) with inactivation removed [21] and the mouse brain Kv1.1 channel (mKv1.1). One chimera, named ShH4-mKv1.1, incorporates the amino-terminal 'sensor' from *Shaker* with the carboxy-terminal 'pore' from mKv1.1. The other chimera, called mKv1.1-ShH4, combines the 'sensor' from mKv1.1 with the 'pore' from *Shaker* (Fig. 1). Functional expression and electro-physiological analysis of the wild type and chimeric channels demonstrate that the modules function outside their native context. We provide a model explaining the equilibrium and kinetic properties of the chimeric channels in terms of the characteristics of the native modules.

2. Materials and methods

2.1. Molecular biology

Standard molecular biological techniques were as described [22]. ShH4-IR [23] was a gift of Ligia Toro (UCLA). The mKv1.1-ShH4 chimera was constructed by replacing the region of mKv1.1 [24] from amino acid 316 onwards with the corresponding residues from *Shaker* H4. Two oligonucleotide primers were used to amplify ShH4-IR from amino acid 345 through the stop codon while simultaneously introducing an *Xho*I site just after the stop codon. The N-terminal portion of mKv1.1 was amplified from before the start codon to residue 315. This piece of mKv1.1 was then cut after nucleotide 377 (amino acid 126) with *Nco*I. The *Nco*I-blunt mKv1.1 fragment and the blunt-*Xho*I ShH4-IR fragment were ligated into the mKv1.1/pGEMHE vector between the *Nco*I site and an *Xho*I site 3′ of the mKv1.1 stop codon. The ShH4-mKv1.1 chimera was constructed by replacing the region of

*Corresponding author. Present address: Plexon Incorporated, 6500 Greenville Avenue Suite 730, Dallas, TX 75206, USA. Fax: (1)-214-369 1775.
E-mail: cdpatten@ucsd.edu

[1] Present address: Università degli Studi di Bologna, Dipartimento di Fisiologia Umana e Generale, Via San Donato 19/2, 40127 Bologna, Italy.
[2] Present address: Centro de Biologia Molecular y Cellular Miguel Hernandez, 03206 Elche (Alicante), Spain.
[3] Present address: Department of Biology, University of California, San Diego, La Jolla, CA 92093, USA.

PII: S0014-5793(99)01659-2

ShH4-IR from amino acid 351 onwards with the corresponding residues of mKv1.1. PCR was used to introduce a silent *Cla*I site in ShH4-IR at amino acids 350–351 and in mKv1.1 at amino acids 321–322. A fragment of mKv1.1 from the *Cla*I site to an *Eco*RV site 3′ of the stop codon was subcloned into ShH4-IR/pBluescript between the *Cla*I site and a blunted *Xho*I site 3′ of the stop codon. The sequences of the transferred segments were verified by both restriction analysis and dideoxy sequencing [25]. For in vitro transcription, ShH4-mKv1.1/pBluescript and mKv1.1-ShH4/pGEMHE DNA were linearized and used as a template. Transcripts of mRNA were prepared using the mMESSAGE mMACHINE kit (Ambion, Austin, TX, USA).

2.2. Electrophysiology

In vitro transcribed RNA was injected into *Xenopus* oocytes as described [26]. Ionic currents were recorded 2–4 days after injection using a two electrode voltage clamp (TEC 10CD, npi electronic, Tamm, Germany) and the Pulse acquisition software (PULSE 8.09, Heka Electronic, Lambrecht, Germany). The oocytes were continually perfused in a barium-containing Ringer's solution: 3.8 mM K^+, 114.2 mM Na^+, 2 mM Ba^{2+}, 10 mM TES, pH 7.4. For tail current measurements, K^+ was raised to 38 mM and Na^+ was lowered to 80 mM. Electrodes were pulled from Corning 7052 glass (Garner Glass, Clairemont, CA, USA) on a P-97 puller (Sutter Instruments, Novato, CA, USA) Electrodes were filled with 1 M KCl buffered with 10 mM TES and typically had resistance less than 500 kΩ. The currents were sampled at 4–5 kHz after filtering at 1 kHz. Leak subtraction was accomplished with two inverted quarter amplitude pre-pulses that were scaled and subtracted from the test pulse. All recordings were made at room temperature, ~21°C.

2.3. Data analysis and modeling

Electrophysiological data were analyzed in the Matlab technical computing environment (Mathworks, Natick, MA, USA) using custom routines. Peak currents were determined by fitting a second order polynomial near the current maximum. Conductance–voltage relationships were characterized in a model-independent way by reporting the potential of half-maximal activation and the true slope (derivative) of the curve at half-maximal activation. The kinetic properties of the channels were initially assessed by looking at the 10% to 90% rise time and the 90% to 10% fall time. To find 10% and 90% level crossings, the currents and levels were displayed on a logarithmic time scale. The intersection of the current with each level was selected manually. For fitting, model parameter minimization was performed using the simplex algorithm as implemented in Matlab ('fmins' function). To avoid problems of local minima, minimizations were repeated from large numbers of random seeds. For the equilibrium model of activation, minimization from 2400 seeds failed to uncover a better fit.

3. Results

3.1. Swapping modules produces functional chimeric channels

To examine the functional significance of the putative modules of the voltage-gated potassium channel, we constructed chimeric channels that were hybrids of the ShH4 and mKv1.1

Table 1
Qualitative description of channel kinetics in terms of module kinetics

	Sensor	Pore	Activation	Deactivation
mKv1.1	1	2	(1) Slow	(2) Slow
mKv1.1-ShH4	1	4	(1) Slow	(4) Fast
ShH4-mKv1.1	3	2	(2) Medium	(3) Medium
ShH4	3	4	(3) Fast	(4) Fast

Each module has been ranked with a speed from 1 to 4 with 1 being the slowest and 4 being the fastest. Since activation requires both modules to enter the permissive state, the rate of activation is limited by the slower of the two modules comprising the channel. Deactivation occurs when either module leaves the permissive state, so the rate of deactivation is determined by the faster of the two modules comprising the channel.

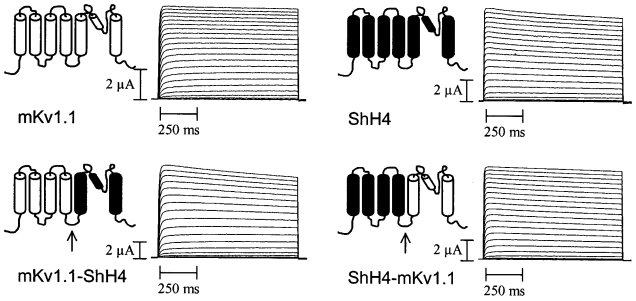

Fig. 1. Expression of chimeric channels in *Xenopus* oocytes. Currents elicited in response to 750 ms depolarizing pulses to test potentials between −70 mV and +50 mV in 5 mV increments from a holding potential of −100 mV. mKv1.1 (mKv1.1), Shaker H4 (inactivation removed), the mKv1.1-ShH4 chimera, and the ShH4-mKv1.1 chimera expressed currents typical of delayed rectifier potassium channels. The maximum current is 6.07 μA for mKv1.1, 8.17 μA for Shaker H4, 10.7 μA for the mKv1.1-ShH4 chimera, and 8.6 μA for the ShH4-mKv1.1 chimera. Two inverted quarter amplitude pulses were used for leak subtraction. Arrows indicate the approximate location of the chimeric joint on the predicted topology of the channels.

potassium channels (see Section 2 and Fig. 1). Wild type *Shaker* H4 and mKv1.1 channels, as well as chimeric ShH4-mKv1.1 and mKv1.1-ShH4 channels, were functionally expressed in *Xenopus* oocytes. As shown in Fig. 1, all four constructs induced the expression of voltage-gated potassium-selective currents in the oocytes that were typical of the class known as delayed rectifier potassium channels. At negative membrane potentials the channels are closed and depolarizing pulses cause the channels to open or activate. The voltage range of activity of the mKv1.1 potassium channel is slightly hyperpolarized from that of the *Shaker* H4 channel. We characterized the currents by looking at the peak conductance–voltage relation (GV) as shown in Fig. 2A. mKv1.1 channels activated at the most negative potentials with a half-activation potential of -26.4 ± 2.1 mV ($n = 17$, mean ± S.D.). *Shaker* H4 channels had a half-activation potential of -14.4 ± 3.9 mV ($n = 22$). The chimeric channels displayed peak conductance–voltage relationships that were distinct from either of the wild type channels. The ShH4-mKv1.1 chimera exhibited a half-activation potential intermediate between mKv1.1 and *Shaker* H4 at -18.2 ± 2.0 mV ($n = 18$). However, the mKv1.1-ShH4 chimera exhibited a large depolarizing shift with a half-activation potential of 3.0 ± 3.7 mV. The half-activation voltages and the slopes of the GV curves are summarized in Fig. 2B.

The kinetic behavior of the *Shaker* H4 channel is also significantly different from that of mKv1.1. *Shaker* channels activate and deactivate much faster than mKv1.1 channels at a given test potential. The rate at which these channels activate and deactivate is also strongly voltage-dependent, with the channels activating much more rapidly at progressively depolarized potentials (Fig. 3C) and deactivating more rapidly at hyperpolarized potentials (Fig. 4C). We quantified the rate of channel activation by measuring the rise time, the time it takes for the current to rise from 10% to 90% of its maximal value following a depolarizing stimulus (Fig. 3A,B). For example, ShH4 channels have a mean rise time of 37 ms at −36 mV but rise in 2.7 ms at +41 mV. At all potentials measured, ShH4 channels activated in the least amount of time (Fig. 3C). mKv1.1 channels take from fourfold longer to activate at highly depolarized potentials (V_{pulse} ~+40 mV) to up to 10

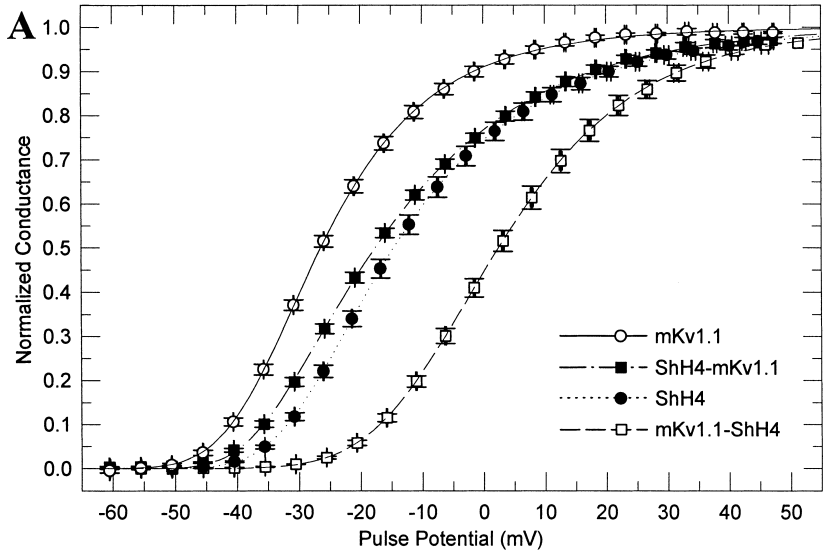

B

	V half (mV)	Slope (%/mV)	n
mKv1.1	-26.4 ± 2.1	2.8 ± 0.5	17
ShH4	-14.4 ± 3.9	2.0 ± 0.2	22
mKv1.1-	3.0 ± 3.7	2.3 ± 0.6	14
ShH4-	-18.2 ± 2.0	2.3 ± 0.5	18

C

	Sensor		Pore		
	ΔG_0	ΔZ	ΔG_0	ΔZ	ΔC
mKv1.1	-1.52	-1.91	-1.15	-1.31	3.22
ShH4	-4.67	-2.95	-2.70	-1.18	0.01
mKv1.1-	-1.52	-1.91	-2.70	-1.18	0.29
ShH4-	-4.67	-2.95	-1.15	-1.31	1.57

Fig. 2. A: Peak conductance–voltage relationships (GVs) with 3.8 mM external potassium. Oocytes were held at −100 mV and depolarized to test potentials from −70 mV to +50 mV in 5 mV increments. The peak current during the pulse was divided by the driving force to obtain the conductance. The conductance was normalized by the maximal conductance in that oocyte before averaging with other oocytes. The reversal potential under these conditions is −81 mV. Conductance symbols are mean ± S.E.M. with the number of oocytes indicated in B. Fitted curves are the prediction of the model described in the text and in C. B: Model-independent characterization of the GVs. The range over which the channels activate is summarized by the half-activation potential and the slope of the GV curve at the half-activation point. The slope is the percent change in activation per millivolt shift away from the half activation potential. For example, at −26.4 mV mKv1.1 channels are 50% activated, and at −26.4+1 = −25.4 mV they are 50+2.8 = 52.8% activated. Values are mean ± S.D. C: Best-fit parameters of the model described in the text. ΔG and ΔC are measured in units of kT and ΔZ is measured in terms of the fundamental charge e. Note that the ΔG and ΔZ values for the chimeras are identical to those of the native channels.

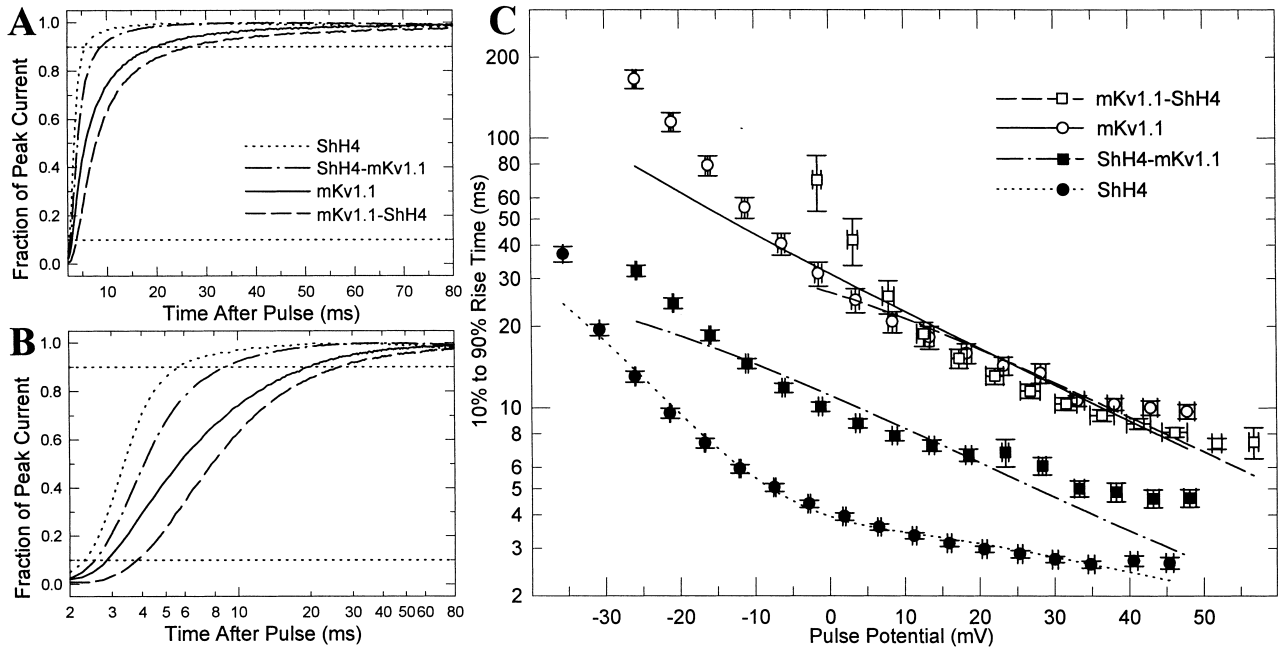

Fig. 3. Activation kinetics of wild type and chimeric channels. A: Time course of normalized current as channels activate during a pulse to +10 mV from a holding potential of −100 mV. We quantified the rate of channel activation by looking at the rise time, the time for the channel to activate from 10% to 90% of its peak. The 10% and 90% activation levels are indicated by the horizontal dotted lines. B: Same currents as in A, but shown with a logarithmic time axis to better visualize the 10% and 90% crossings. C: The rise time as a function of the pulse potential. Rise time decreases dramatically with increased depolarization. Notice that the vertical time axis is logarithmic. Rise time symbols represent the mean rise time ± S.E.M. Fitted curves are the prediction of the model described in the text. The transition state energy barriers were 24.94, 24.00, 22.92 and 22.69 kT for the mKv1.1 sensor, mKv1.1 pore, ShH4 sensor, and ShH4 pore respectively. The charge carried by these transitions was −0.77, −0.75, −0.33, and −1.65 charges respectively.

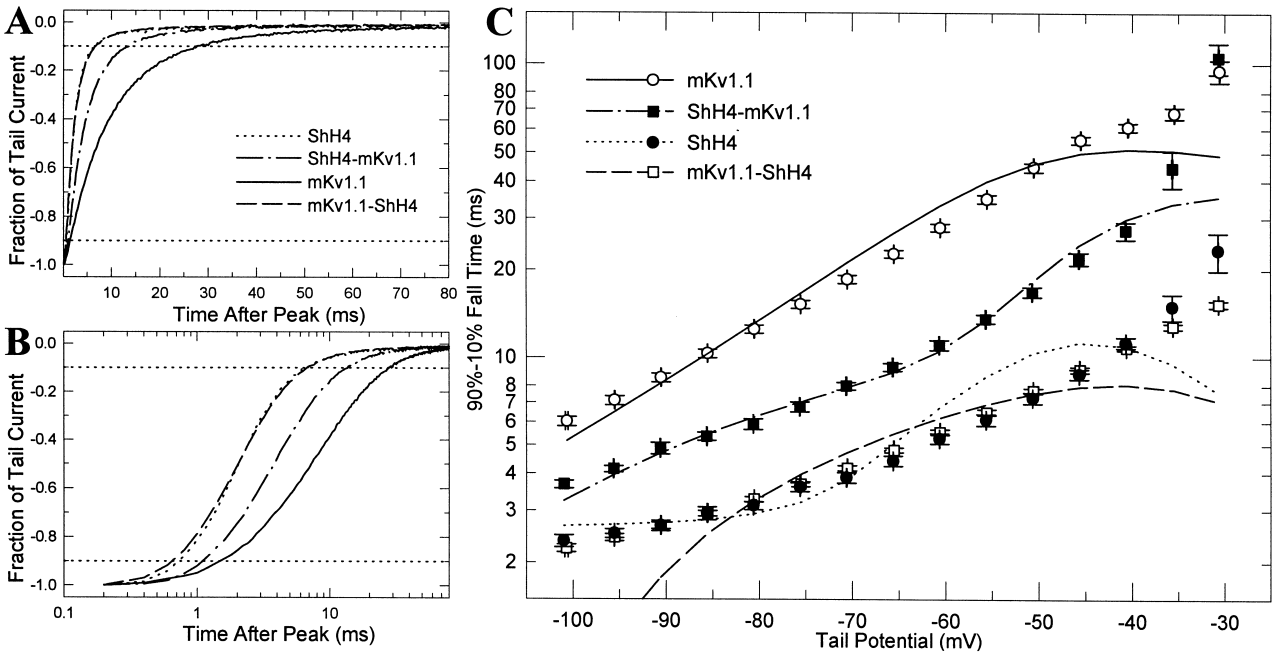

Fig. 4. Deactivation kinetics. Tail currents were measured with 38 mM external potassium. A: Inward tail currents in response to repolarizing the membrane to −60 mV after a depolarization to +20 mV. The tail currents have been normalized to their maximum value. To quantify the rate of deactivation (closing) we measured the fall time, the time it takes for the tail current to decay from 90% to 10% of its maximal value. The horizontal dotted lines indicate the 90% and 10% levels. B: Same tail currents as in A, but plotted with a logarithmic time scale to better resolve the 90% and 10% level crossings. Notice that the ShH4 tail current (dotted line) and the mKv1.1-ShH4 (dashed line) are essentially overlapping. C: Fall time as a function of repolarization potential. Channels deactivate rapidly at hyperpolarized potentials and the fall time increases exponentially with depolarization. Fall time symbols represent the mean fall time ± S.E.M. Fitted curves are the prediction of the model described in the text.

times longer to activate at less depolarized potentials (V_{pulse} ∼−20 mV). The mKv1.1-ShH4 chimera has a rise time that is comparable to that of mKv1.1 at potentials above +10 mV suggesting that the mKv1.1 sensor module at these potentials kinetically limits activation of the channels. Finally, the ShH4-mKv1.1 chimera has a rise time that is intermediate between those of ShH4 and mKv1.1.

To quantify the rate of channel deactivation or closing, we measured the fall time, the time it takes for inward tail currents to decay from 90% to 10% of their peak values (Fig. 4A,B). Tail current decay was most rapid at hyperpolarized potentials and slowed exponentially with depolarization (Fig. 4C). Again, ShH4 channels exhibited the most rapid kinetics. However, the fall times were virtually identical for the mKv1.1-ShH4 chimera and the wild type ShH4 channel (Fig. 4C), suggesting that the ShH4 pore module determines the deactivation kinetics of these channels. Tail currents from ShH4 and mKv1.1-ShH4 had fall times of 2.4 ms and 2.2 ms respectively at −101 mV, and fall times of 11.3 ms and 10.8 ms respectively at −41 mV. mKv1.1 channels had the slowest deactivation kinetics, exhibiting fall times from 6.0 ms at −101 mV to 61.2 ms at −40 mV. Thus mKv1.1 deactivates 2.5–5 times more slowly than *Shaker*. The deactivation kinetics of the ShH4-mKv1.1 chimera were intermediate between those of ShH4 and mKv1.1.

3.2. Functional modeling of chimeras at equilibrium

To explain the equilibrium properties of the chimeric channels, we designed a functional model. The model considers the channel to be composed of four subunits in view of the tetrameric stoichiometry of voltage-gated potassium channels [27,28]. Each subunit is composed of two modules: one sensor module (S) and one pore module (P). Each module in turn has two functional states, one of which is permissive to channel opening (S^+ or P^+) and one of which is not (S^- or P^-). In order for the channel to open, both modules of each subunit must be in the permissive state. At zero membrane potential, there is a free energy difference between the permissive and non-permissive states, ΔG_0. Voltage dependence is accounted for by charge movement across the membrane, ΔZ, as the module moves from its non-permissive to permissive states (Fig. 5A). To account for communication between the sensor module and the pore module, there is a coupling energy, ΔC, between the two modules when they are both in their permissive states (Fig. 5B). Finally, the probability that a module is in a given state at equilibrium is governed by the Boltzmann distribution, so the probability of any state is inversely related to the exponential of its energy (Fig. 5C).

The important feature of this model is that the properties of any module (ΔG_0 and ΔZ) are invariant regardless of whether the module is part of the native channel or incorporated into a chimeric channel. Therefore, the coupling energy between the particular sensor and pore module in a given construct is the only property unique to that particular channel. Minimization of the model yielded a set of module properties (Fig. 2C) which described the conductance voltage relationships of mKv1.1, *Shaker* H4, and the two chimeras quantitatively (Fig. 2A).

3.3. Kinetic modeling of chimeras

To accommodate kinetics of the channels, we introduced a transition state between the permissive and non-permissive

states of each module. The transition state was characterized by its free energy (ΔG_{ST} or ΔG_{PT}, Fig. 6A) which was voltage-dependent. Transition rates between the states of each subunit were then assigned according to the energy barrier presented by the transition state (Fig. 6B). Rise times and fall times were calculated from the model using the Q-matrix method [29] (Fig. 6C). The rise times and fall times predicted by the model are shown in Figs. 3C and 4C respectively. Because computation of the predicted rise and fall times is complex, it is useful to consider the kinetic predictions of the model from a qualitative perspective (Table 1). The activation kinetics of mKv1.1 and mKv1.1-ShH4 can be described as slow, those of ShH4-mKv1.1 as medium, and those of ShH4 as fast (Fig. 3C, Table 1). Likewise, the deactivation kinetics of mKv1.1 can be described as slow, those of ShH4-mKv1.1 as intermediate, and those of ShH4 and mKv1.1-ShH4 as fast (Fig. 4C, Table 1).

Activation requires both modules to enter into their permissive states before the channel can open. This is similar to the notion that the voltage-gated potassium channels have two gates [30]. The rate of activation will therefore be limited by the slower of the two modules. Meanwhile deactivation can occur if either of the modules leaves the permissive state.

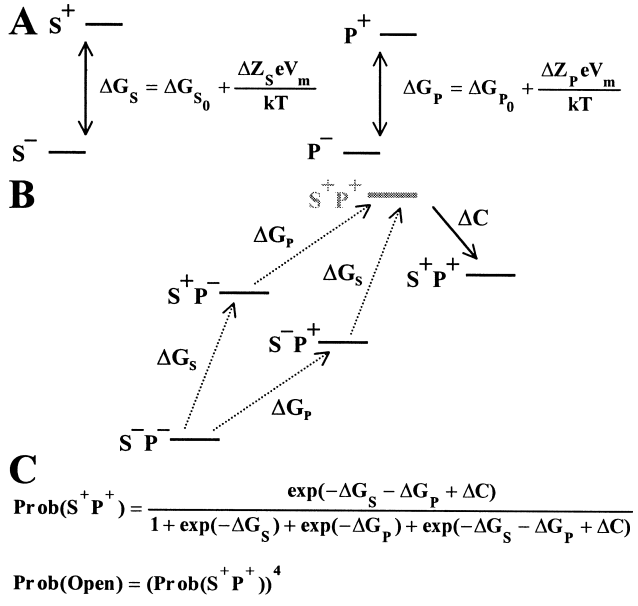

Fig. 5. Equilibrium model of chimeric channels. Each of the four subunits of the channel is composed of two modules: a sensor, S, and a pore, P. A: Each module has two states, one which is permissive to channel opening, labeled +, and one which is not, labeled −. These two states are separated by a free energy difference ΔG which varies with the membrane potential V_m. The properties of a given module are invariant regardless of whether the module is part of a wild type or chimeric construct. B: Each subunit thus has four states, S^-P^-, S^+P^-, S^-P^+, and S^+P^+. When the two modules are both in their permissive states they experience a favorable interaction that stabilizes the S^+P^+ state by an energy ΔC which is voltage-independent. C: The probability of a subunit being in a given state is determined by the Boltzmann distribution. Since the channel is composed of four independent subunits, the probability of channel opening is equal to the probability that one subunit is in the S^+P^+ state raised to the fourth power. Since ΔG_S and ΔG_P are functions of voltage, so is the open probability. The simultaneous fit of this model to the four conductance voltage relationships is shown in Fig. 2.

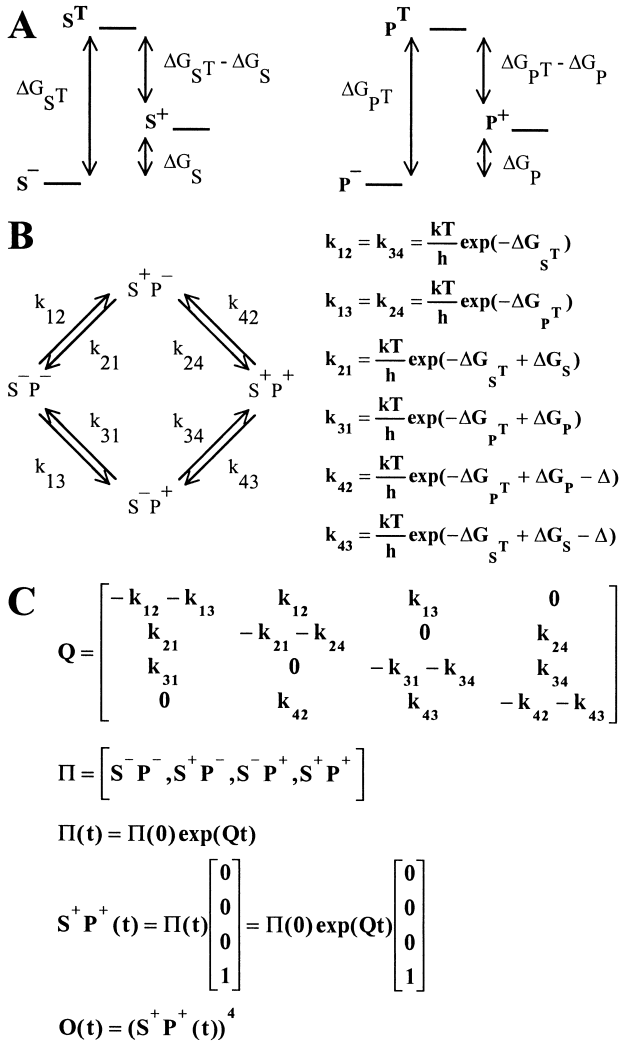

Fig. 6. Kinetic model of channel activation. A: Addition of a transition state between the permissive and non-permissive states of each module permits kinetic predictions. The transition state energy is voltage-dependent and is not drawn to scale. B: Kinetic scheme for one subunit. The transition rates are calculated using Erying rate theory. Because the S^+P^+ state is favorably stabilized, the exit rates from this state, k_{43} and k_{42}, are slowed (see text). C: Q-matrix of the kinetic scheme in B. We used the Q-matrix formalism to calculate the time course of activation, and hence the rise time. Π is a vector of probabilities that the subunit is in a particular state. $\Pi(0)$ is the equilibrium probability distribution of the subunit at the holding potential. Because the channel is composed of four independent subunits, the time course of channel opening is equal to the time course of arriving in the S^+P^+ state raised to the fourth power.

Therefore, the rate of deactivation will be determined by the faster of the two modules. Consider replacing the *Shaker* pore in ShH4 with the pore from mKv1.1 to create the ShH4-mKv1.1 chimera. This modification slows activation (Fig. 3). We can conclude that the mKv1.1 pore module is kinetically slower than the ShH4 pore module. This modification also slows deactivation. From this we can conclude that the ShH4 sensor module is slower than the ShH4 pore module. If the reverse were true and the ShH4 pore module were faster than the sensor module, then we would not expect deactivation to be slowed by the mKv1.1 pore module. Using similar logic, we can rank the speed of the various modules as shown

in Table 1. The kinetic properties of the chimeric channels then follow directly from the kinetic properties of the individual modules. This qualitative ranking is supported by the transition state energy barriers of the model: the mKv1.1 sensor module has the highest transition state energy (Fig. 3 legend) and is thus the slowest module while the ShH4 pore module has the lowest transition state energy and is thus the fastest module. The quantitative kinetic predictions of the model (Figs. 3C and 4C) do not exactly match the observed rise and fall times of every construct at every potential. However, we have deliberately chosen a minimal model with only those parameters necessary to demonstrate the concept of channel modularity. Considering the simplicity of the model, the kinetic predictions are surprisingly good and the equilibrium predictions are excellent.

4. Discussion

Chimeric constructs were initially used to probe the permeation and pharmacology of potassium channels [31–34] and the kinetics of calcium channels [35,36]. More recently, the voltage-dependent gating of potassium channels has been assessed with chimeric constructs involving the exchange of single transmembrane segments or loops. Chimeric channels in which the S4 segment [37–39], the S5 segment [40], or the S3-S4 loop [41] have been replaced show that multiple regions of the protein contribute to the determination of the voltage-dependent gating of the channel. Here we have assembled functional chimeric voltage-dependent potassium channels which demonstrate that the N-terminal portion of the channel up to and including the S4 transmembrane segment and the C-terminal portion of the channel including S5, H5, and S6 can function as exchangeable modules. We propose a novel type of intrasubunit cooperativity between these modules. Our model assigns invariant functional properties to these modules and explains the properties of fully assembled channels in terms of the characteristics of the modules from which they are built.

There are a number of interesting features of the model that merit discussion. The total number of charges per channel is 12.9 for mKv1.1 and 16.5 for ShH4, values that are in agreement with current estimates of charge movement in voltage-gated potassium channels [42]. Notice, however, that the slope of the peak conductance versus voltage curve (GV curve) (Fig. 2B) is steeper for mKv1.1 than for ShH4. This is an excellent demonstration that the slope of the GV curve is a poor indicator of charge movement during channel activation. Rather, the increased slope of the mKv1.1 GV curve results from the intrasubunit cooperative interaction between the mKv1.1 sensor and pore modules. The coupling energy between the sensor and pore modules was 3.22 kT for mKv1.1 and approximately half of this, 1.57 kT, for the ShH4-mKv1.1 chimera. Meanwhile our model showed very little interaction between the modules of the ShH4 or mKv1.1-ShH4 channels. This suggests that the mKv1.1 pore module exerts a positive feedback on the sensor module to which it is attached. It will be interesting to probe the mechanism of this interplay between modules using site-directed mutagenesis.

For both ShH4 and mKv1.1, the majority of the charge movement is associated with the sensor module as expected: 71% for ShH4 and 60% for mKv1.1. It would be interesting to examine if inward rectifier channels constructed from the pore modules of these channels (cf. [43]) exhibit slight voltage dependence consistent with the charge we have assigned to them.

Our kinetic measurements show that mKv1.1 channels are kinetically much slower than ShH4 channels in both activation and deactivation. Furthermore our model suggests that mKv1.1 channels carry less gating charge per channel than ShH4. Both of these features could significantly reduce the amplitude of mKv1.1 gating currents relative to ShH4 gating currents. We have observed that mKv1.1 gating currents are indeed much smaller than those of ShH4 are (B. Tam and M. Montal, unpublished observations).

An interesting application of this modular design strategy will be to generate chimeric channels that incorporate the *Shaker* pore module and the W434F mutation which renders *Shaker* potassium channels non-conducting. Constructs with a non-conducting pore module will be useful for measuring gating currents from channels in which the mutation corresponding to W434F is not effective (or in which there is no corresponding residue). Such constructs should prove useful in elucidating the mechanism by which W434F renders the *Shaker* channel non-conducting. It could act by occluding the pore or by disrupting the coupling between sensor and pore modules (cf. [44]).

We have shown that the equilibrium and kinetic properties of the chimeric channels ShH4-mKv1.1 and mKv1.1-ShH4 can be explained in terms of the characteristics of the modules from which they are constructed. Therefore these channels are both structurally and functionally modular.

Acknowledgements: We would like to thank L. Toro for the Shaker H4-IR clone, E.R. Liman for the pGEMHE vector, and B.M. Patten for reading the manuscript. This work was supported by U.S. Public Health Service Grants GM49711 and GM56538 and by a Training Grant, 5T32 GM08326, from the National Institutes of General Medical Science.

References

[1] Tempel, B.L., Papazian, D.M., Schwarz, T.L., Jan, Y.N. and Jan, L.Y. (1987) Science 237, 770–775.
[2] Noda, M., Shimizu, S., Tanabe, T., Takai, T., Kayano, T., Ikeda, T., Takahashi, H., Nakayama, H., Kanaoka, Y., Minamino, N., Kangawa, K., Matsuo, H., Raftery, M.A., Hirose, T., Inayama, S., Hayashida, H., Miyata, T. and Numa, S. (1984) Nature 312, 121–127.
[3] Tanabe, T., Takeshima, H., Mikami, A., Flockerzi, V., Takahashi, H., Kangawa, K., Kojima, M., Matsuo, H., Hirose, T. and Numa, S. (1987) Nature 328, 313–318.
[4] Montal, M. (1995) Annu. Rev. Biophys. Biomol. Struct. 24, 31–57.
[5] Montal, M. (1996) Curr. Opin. Struct. Biol. 6, 499–510.
[6] Jan, L.Y. and Jan, Y.N. (1997) Annu. Rev. Neurosci. 20, 91–123.
[7] Ho, K., Nichols, C.G., Lederer, W.J., Lytton, J., Vassilev, P.M., Kanazirska, M.V. and Hebert, S.C. (1993) Nature 362, 31–38.
[8] Schrempf, H., Schmidt, O., Kümmerlen, R., Hinnah, S., Müller, D., Betzler, M., Steinkamp, T. and Wagner, R. (1995) EMBO J. 14, 5170–5178.
[9] Doyle, D.A., Cabral, J.M., Pfuetzner, R.A., Kuo, A., Gulbis, J.M., Cohen, S.L., Chait, B.T. and MacKinnon, R. (1998) Science 280, 69–77.
[10] Papazian, D.M., Timpe, L.C., Jan, Y.N. and Jan, L.Y. (1991) Nature 349, 305–310.
[11] McCormack, K., Tanouye, M.A., Iverson, L.E., Lin, J., Ramaswami, M., McCormack, T., Campanelli, J.T., Mathew, M.K. and Rudy, B. (1991) Proc. Natl. Acad. Sci. USA 88, 2931–2935.
[12] Lopez, G.A., Jan, Y.N. and Jan, L.Y. (1991) Neuron 7, 327–336.
[13] Liman, E.R., Hess, P., Weaver, F. and Koren, G. (1991) Nature 353, 752–756.

[14] Logothetis, D.E., Movahedi, S., Staler, C., Lindpaintner, K. and Nadal-Ginard, B. (1992) Neuron 8, 531–540.
[15] Greenblatt, R.E., Blatt, Y. and Montal, M. (1985) FEBS Lett. 193, 125–134.
[16] Montal, M. (1990) FASEB J. 4, 2623–2635.
[17] Planells-Cases, R., Ferrer-Montiel, A.V., Patten, C.D. and Montal, M. (1995) Proc. Natl. Acad. Sci. USA 92, 9422–9426.
[18] Seoh, S., Sigg, D., Papazian, D.M. and Bezanilla, F. (1996) Neuron 16, 1159–1167.
[19] Ketchum, K.A., Joiner, W.J., Sellers, A.J., Kaczmarek, L.K. and Goldstein, S.A.N. (1995) Nature 376, 690–695.
[20] Lesage, F., Guillermare, E., Fink, M., Duprat, F., Lazdunski, M., Romey, G. and Barhanin, J. (1996) EMBO J. 15, 1004–1011.
[21] Hoshi, T., Zagotta, W.N. and Aldrich, R.W. (1990) Science 250, 533–538.
[22] Sambrook, J., Fritsch, E.F. and Maniatis, T. (1989) Molecular Cloning: A Laboratory Manual, 2nd edn., Cold Spring Harbor Laboratory Press, Cold Spring Harbor, NY.
[23] Stefani, E., Toro, L., Perozo, E. and Bezanilla, F. (1994) Biophys. J. 66, 996–1010.
[24] Ferroni, S., Planells-Cases, R., Ahmed, C.M.I. and Montal, M. (1992) Eur. Biophys. J. 21, 185–191.
[25] Sanger, F., Nicklen, S. and Coulson, A.R. (1977) Proc. Natl. Acad. Sci. USA 74, 5463–5467.
[26] Ferrer-Montiel, A.V. and Montal, M. (1994) Methods Companion Methods Enzymol. 6, 60–69.
[27] MacKinnon, R. (1991) Nature 350, 232–235.
[28] Liman, E.R., Tytgat, J. and Hess, P. (1992) Neuron 9, 861–871.
[29] Fredkin, D.R., Montal, M. and Rice, J.A. (1985) in: Proceedings of the Berkeley Conference in Honor of Jerzy Neyman and Jack Kiefer (LeCarn, L.M. and Olshen, R.A., Eds.), Vol. 1, pp. 269–289, Wadsworth, Monterey, CA.
[30] Liu, Y. and Joho, R. (1998) Pflügers Arch.-Eur. J. Physiol. 435, 654–661.
[31] Hartmann, H.A., Kirsch, G.E., Drewe, J.A., Taglialatela, M., Joho, R.H. and Brown, A.M. (1991) Science 251, 942–944.
[32] Goulding, E.H., Tibbs, G.R., Liu, D. and Siegelbaum, S.A. (1993) Nature 364, 61–64.
[33] Taglialatela, M., Champagne, M.S., Drewe, J.A. and Brown, A.M. (1994) J. Biol. Chem. 269, 13867–13873.
[34] Cao, Y., Crawford, N.M. and Schroeder, J. (1995) J. Biol. Chem. 270, 17697–17701.
[35] Tanabe, T., Adams, B.A., Numa, S. and Beam, K.G. (1991) Nature 352, 800–803.
[36] Nakai, J., Adams, B.A., Imoto, K. and Beam, K.G. (1994) Proc. Natl. Acad. Sci. USA 91, 1014–1018.
[37] Logothetis, D.E., Kammen, B.F., Lindpainter, D., Bisbas, D. and Nadal-Ginard, B. (1993) Neuron 10, 1121–1129.
[38] Koopmann, R., Benndorf, K., Lorra, C. and Pongs, O. (1997) Receptors Channels 5, 15–28.
[39] Smith-Maxwell, C.J., Ledwell, J.L. and Aldrich, R.W. (1998) J. Gen. Physiol. 111, 399–420.
[40] Shieh, C., Klemic, K.G. and Kirsch, G.E. (1997) J. Gen. Physiol. 109, 767–778.
[41] Tang, C. and Papazian, D.M. (1997) J. Gen. Physiol. 109, 301–311.
[42] Noceti, F., Baldelli, P., Wei, X., Qin, N., Toro, L., Birnbaumer, L. and Stefani, E. (1996) J. Gen. Physiol. 108, 143–155.
[43] Tytgat, J., Vereecke, J. and Carmeliet, E. (1994) J. Physiol. 481, 7–13.
[44] Yang, Y., Yan, Y. and Sigworth, F.J. (1997) J. Gen. Physiol. 109, 779–789.